Impacts of topography change on saltwater intrusion over the past decade in the Changjiang Estuary

Qing Chen[a,c], Jianrong Zhu[a,b,*], Hanghang Lyu[a] , Shunqi Pan[c], Shenliang Chen[a,b]

[a] State Key Laboratory of Estuarine and Coastal Research, East China Normal University, Shanghai, 200062, PR China

[b] Shanghai Institute of Eco-Chongming, Shanghai, 200062, PR China

[c] Hydro-environmental Research Centre, School of Engineering, Cardiff University, Cardiff CF24 3AA, UK

Correspondence should be addressed to Jianrong Zhu

E-mail address: jrzhu@sklec.ecnu.edu.cn

Abstract

Saltwater intrusion in estuaries is mainly controlled by tides and river discharge, as well as by topography and other factors. The Changjiang estuary has been seen a significant change in its topography from the data obtained in 2007 and 2017. In this study, a well-validated 3D numerical model was used to simulate and analyze the residual water and salt transport, water diversion ratio (WDR) in bifurcated channels and water resources in the Changjiang Estuary in 2007 and 2017. The comparisons of the model results showed that due to the North Branch becoming much shallower and narrower over the period from 2007 to 2017, the overall salinity in the North Branch decreased and the intensity of saltwater spillover (SSO) from the North Branch into the South Branch weakened. In the North Channel, the simulated residual or net transection water flux (NTWF) and WDR decreased during spring tides, resulting in increased saltwater intrusion. During neap tides, the saltwater intrusion was weakened despite the decreased NTWF and WDR because the water depth at the river mouth became shallower. The changes of topography during that period also resulted in changes of DWR, NTWF, salt transport across the tidal flats and dykes in the North Passage, South Passage and the South Channel, as well as overall dynamic mechanism. The results indicated that the salinity at the water intakes of the three reservoirs in the estuary slightly decreased, indicating that the time that reservoirs can take water from the estuary become longer in dry seasons. In the scenario of complete silt-up of the North Branch, the saltwater intrusion was weakened in the South Branch because of the disappearance of the SSO, which was favorable for the utilization of freshwater resources, but enhanced in the North Channel, North and South Passages. The overall influence from the topographic change over the period is that the saltwater intrusion is weakened in the North Branch, and enhanced during spring tides and weakened during neap tides in the North

Channel, North and South Passages. Sediment accretion in the North Branch is favorable for utilization of freshwater resources.

Keywords: topography change; saltwater intrusion; freshwater resource; numerical model; Changjiang Estuary.

1. Introduction

Saltwater intrusion is a common phenomenon in estuaries where freshwater and saltwater converge. Saltwater intrusion can produce estuarine circulation (Pritchard, 1956) and affect stratification (Simpson et al., 1990), thereby influencing sediment transport, producing peak estuarine turbidities (Geyer, 1993), and degrading freshwater quality (Zhu et al., 2010). Estuarine saltwater intrusion is mainly controlled by tide and river runoff (Pritchard, 1956; Prandle, 1985; Shen et al., 2003), but it can also be affected by topography (Prandle, 2006), wind stress (Hansen and Rattray, 1966; Li et al., 2012), and vertical mixing (Ippen and Harleman, 1961; Simpson and Hunter, 1974; Prandle and Lane, 2015). Prandle (2006) presented the relation between the estuarine morphological development and the forcing parameters such as tide range and river flow with the data from 80 UK estuaries. It can be well explained from these theoretically derived relationships and indicated that estuarine topography evolution should be considered in the determination of saline intrusion length. Estuarine topographies reflected the influences of tidal amplitude and river flow, along with some representation of alluvium (Prandle and Lane, 2015). Topography change was caused by natural evolution over long time scales and anthropogenic activities, especially in recent decades (Shen et al., 2003; Zhu and Bao, 2016).

Changjiang, also known as the Yangtze River, is one of the largest rivers in the world. The river discharges large amounts of freshwater (9.24×10^{11} m^3) into the East China Sea each year (Shen et al., 2003). The seasonal variation of river discharge ranges from a maximum monthly mean of 49,850 m^3s^{-1} in July to a minimum of 11,180 m^3s^{-1} in January (Zhu et al., 2015). The estuary has a 90-km-wide river mouth and a nearly 640-km tidal limit. The Changjiang Estuary is characterized by multiple bifurcations (Fig. 1). The estuary is first divided into the South

Branch (South Branch) and the North Branch (North Branch) by Chongming Island. The lower South Branch was then bifurcated into the South Channel (South Channel) and the North Channel (North Channel) by Changxing Island and Hengsha Island. The South Channel was again bifurcated into the South Passage and the North Passage by the Jiuduan Sandbank. In 2017, the mean water depths in the North Branch, South Branch, North Channel, South Channel, and North and South Passages were 4.27, 10.41, 8.34, 11.47, 7.22 and 5.75 m, respectively. Tides in the Changjiang Estuary are semidiurnal, and fortnightly spring-neap signals and the most energetic source of water movement, which are close to a mesoscale. The maximum spring tide range was 3.38 m and the minimum neap tide range was 0.64 m at the Baozhen hydrological station (Fig. 1b) (Zhu, et al., 2015). The maximum tidal current amplitudes reached approximately 2.0 m/s at the river mouth during spring tide. The prevailing monsoon climate resulted in a stronger northerly wind of 5.5 m/s during winter and a southeasterly wind of 5.0 m/s during summer (Zhu, et al., 2015). The northerly wind produced a southward current along the Jiangsu coast in winter, which resulted in a higher water level along the coast by the Ekman transport. So the northerly wind caused a horizontal circulation around the Changjiang Estuary, which flowed into the estuary in the North Channel and out of the estuary in the South Channel (Wu et al., 2010; Li et al., 2012).

River discharge and tides are major control factors of saltwater intrusion in the Changjiang Estuary (Li et al., 2010; Qiu et al., 2012; Shen et al., 2003; Wu et al., 2006; Zhu et al., 2010;) but is also influenced by wind (Li et al., 2012), topography (Li, et al., 2014), anthropogenic activities in the river basin and estuary (Lyu and Zhu, 2018a; Qiu and Zhu, 2013; Zhu, et al., 2006) and sea-level rise (Qiu and Zhu, 2015). The North Branch is always found to be filled with highly saline water due to a low river discharge and high tidal range. In addition, saltwater intrusion is

found to be the strongest in the South Passage and the weakest in the North Channel, mainly in a landwards wedge-like manner, especially during neap tide, similar to those observed in other partially mixed estuaries (Shen et al., 2003). During the dry seasons, when the river discharge is low, the North Branch always contains highly saline water under strong tidal conditions and low river discharge. Due to the bifurcation nature of the estuary, there is a particular type of saltwater intrusion in Changjiang Estuary compared with the other estuaries in the world, which is known as saltwater spillover (SSO) from the North Branch into the South Branch, and the SSO commonly occurs during spring tides of the dry seasons (Shen et al., 2003; Wu et al., 2006; Wu and Zhu, 2007; Wu et al., 2010; Zhu et al., 2016), which are defined as the period from November to March (next year) when the river discharge is usually low. Only a small amount of the saltwater returns to the North Branch because the shoals in its upper reaches surface during ebb tides. The saline water from the SSO during spring tides is transported downstream by runoff during the subsequent middle tides and neap tides. This pattern of saltwater intrusion poses a significant threat to the security of freshwater resources stored in three reservoirs in the estuary: Qingcaosha Reservoir (QCSR), Chenhang Reservoir (CHR) and Dongfengxisha Reservoir (DFXSR) (Table 1). The capacity The QCSR is the largest among them and is located in the North Channel, along the northwestern coast of Changxing Island (shown in Fig. 1). The QCSR supplies more than 70% of the freshwater for city Shanghai. But the QCSR is frequently influenced by saltwater intrusion particularly during the dry seasons. The current regulations prevent these reservoirs from taking water from the Changjiang when the salinity is more than 0.45 psu, to meet the standard for drinking water. For convenience of understanding the more acronyms in this paper, the acronyms and their corresponding full names were listed in the Appendix 1.

Table 1

The capacity, daily supply and their feeding population of three reservoirs.

Reservoir	Capacity ($\times 10^4$ m^3)	Daily supply ($\times 10^4$ t/day)	Population ($\times 10^4$)
QCSR	52400	500	1300
CHR	956	130	300
DFXSR	976	15	82

Previous studies on the impacts of topography change on saltwater intrusion in the Changjiang Estuary include the works of Chen and Zhu (2014a) and Lyu and Zhu, 2018a. Li et al. (2014) calculated the differences in saltwater intrusion in the northern outlet of the North Channel in the Changjiang Estuary using different topographic data. Zhu and Bao (2016) calculated the evolution of saltwater intrusion in the Changjiang Estuary in 1950s, 1970s and 2010s. Despite of those studies, the impacts of topography change on saltwater intrusion in the Changjiang Estuary in the recent years have received a little attention. The aim of this study is to bridge the knowledge gap and gain further understanding of the impacts of topography change on estuarine saltwater intrusion and provide a reference to explain similar phenomena in other estuaries.

To study estuarine saltwater intrusion, theoretical method is commonly used to obtain analytic solutions from simplified partial differential equations, i.e., the linear momentum equation of a dynamic balance between horizontal pressure gradient and vertical turbulent viscosity stress, equations for conservation of water and salt in steady state. There are many theoretical studies on the relation between the saltwater intrusion and stratification and vertical mixing in estuaries. For example, Ippen and Harleman (1961) demonstrated that vertical mixing could be related to energy considerations and defined a stratification number that is a ratio of energy dissipation to gain potential energy. Afterwards, Ippen (1966) modified the stratification

number of the available tidal energy (effective in mixing) to that required to mix river and seawater within the saline intrusion length, which is proportional to the square of the water depth. In the same year, Hansen and Rattray (1966) discussed the correlation between the vertical variations in mean velocity and salinity and the role of this correlation in maintaining the steady-state salinity distribution in estuaries where turbulent mixing results primarily from tidal currents. It indicated the variation of water depth would have significant impact on salinity vertical mixing in an estuary. Moreover, some theoretical studies showed that the variation of water depth would also affected the estuarine horizontal mixing. Ippen (1966) proposed the length of an arrested saline wedge based on residual velocity profiles for a stratified estuary, which is a function of water depth, residual velocity, difference in density between bed and surface, and a parameter that varies with river conditions. Prandle and Lane (2015) deduced an explicit expression for saline intrusion length, which shows the river mouth depth is proportional to the saline intrusion length. They also addressed the question of how tidally dominated estuaries would adapt to increases in mean sea level. It was concluded that a mean sea-level rise would have a significant impact in shallow microtidal estuaries.

Review of previous studies suggested that, the estuarine topography change would have a great influence on saltwater intrusion in the horizontal and vertical directions. Whilst the referred theoretical studies could quantify the change of saltwater intrusion in the single-channel estuaries, given that the Changjiang Estuary is a multi-bifurcated channel with complex topography and there exists the complicated SSO, it makes it much more difficult to obtain an analytic solution to reflect the real temporal and spatial variations in saltwater intrusion. Nonlinear interactions between the river discharge, tide, wind stress and topography should be included in investigating the complicated patterns of saltwater intrusion in the estuary. It therefore becomes necessary to

164 employ and advanced 3D numerical model with the capability of solving the primitive equations
165 in this study to simulate the impacts of topography changes from 2007 to 2017 on saltwater
166 intrusion and water resources and capture the variation of hydrodynamics from natural forcing
167 and human activities during this period.

168 In the following sections, the topography changes from 2007 to 2017, and numerical
169 model set up and validation are described, followed by the analysis and comparisons of the
170 water and salt transport, water diversion ratio (WDR), and saltwater intrusion in the estuary.
171 The saltwater intrusion is also predicted under in the scenario that the North Branch is
172 completely silt-up and the conclusions are presented finally.

173

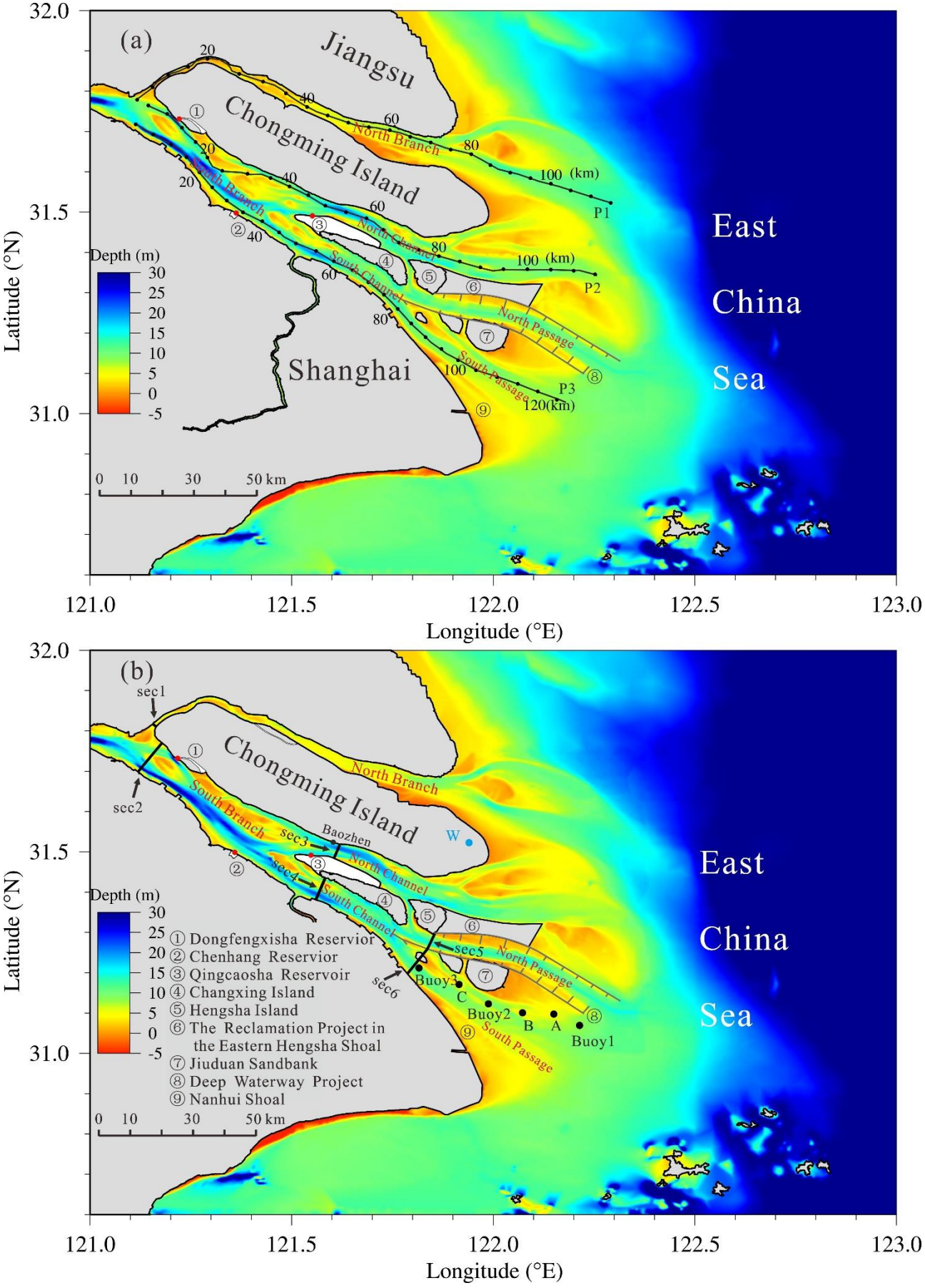

Fig. 1. The measured topographies of the Changjiang Estuary in 2007 (a) and 2017 (b), in

which: A, B and C are ship measurement sites; Buoys 1-3 are buoy measurement locations; Red dots are locations of water intakes of three reservoirs; sec1-sec6 and P1-P3 are cross-sectional longitudinal sections for saltwater intrusion analysis; and W is the location of the weather station.

2. Methods

2.1 Topographic data

In this study, the topographic data as shown in Fig. 1, was sourced from the State Key Laboratory of Estuarine and Coastal Research, surveyed in 2007 and 2017 which reflect the changes in topography over that period.

2.2 Model Setup

To investigate the impacts of topography change on saltwater intrusion in the Changjiang Estuary over period from 2007 to 2017, a well calibrated 3D numerical model was used. The numerical model was based on ECOM-si (Blumberg 1994) and later improved by Chen et al. (2001) and Zhu (2003) for studying hydrodynamics and substance transport. The HSIMT-TVD (high-order spatial interpolation at the middle temporal level coupled with a total variation diminishing scheme limiter) of the advection scheme was developed to significantly reduce the numerical diffusions with third-order accuracy (Wu and Zhu, 2010). The Mellor-Yamada 2.5 order turbulence closure module (Mellor and Yamada, 1982) with stability parameters from Kantha and Clayson (1994) was included. The model used a sigma coordinate system in the vertical direction and a curvilinear non-orthogonal grid in the horizontal direction (Chen et al., 2004). A wet/dry scheme was included to describe the intertidal area with a critical depth of 0.2 m (Zheng et al., 2003; Zheng et al., 2004).

The computational domain of the model for this study covers the Changjiang Estuary and

its adjacent sea (Fig. 2), from 117.5°E to 124.9°E and from 33.7°N to 27.5°N. The model grid was composed of 337 × 225 curvilinear cells horizontally and 10 uniform σ levels vertically. The minimal grid resolution reaches nearly 100 m in the bifurcation of the South Branch and North Branch to better simulate the SSO (Fig. 2). The resolution was relaxed to ~ 10 km near the open boundary.

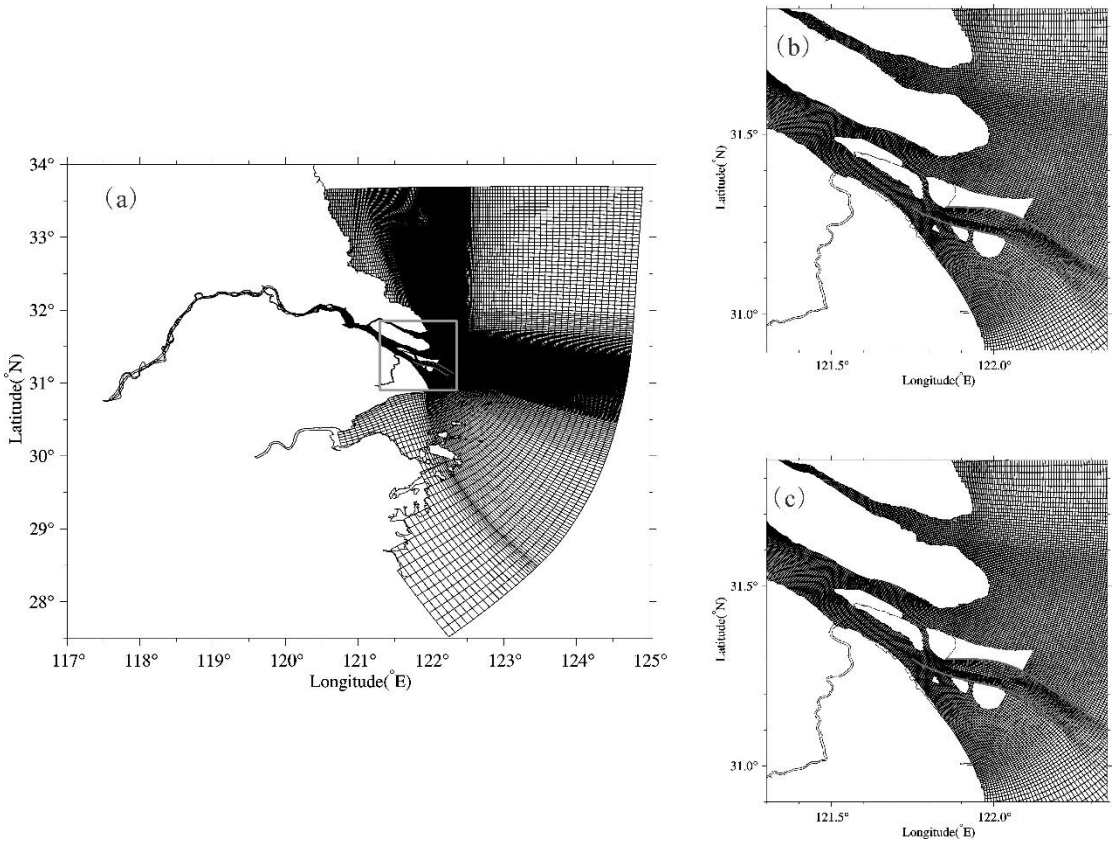

Fig. 2. Numerical model grid (a) and the detailed model grid around the Changjiang Estuary in 2007 (b) and 2017 (c)

Along the open sea boundary of the model, the tide was specified with the 16 astronomical tidal constituents (M_2, S_2, N_2, K_2, K_1, O_1, P_1, Q_1, MU_2, NU_2, T_2, L_2, $2N_2$, J_1, M_1, and OO_1), derived from the NaoTide dataset (https://www.miz.nao.ac.jp/staffs/nao99/). Monthly mean river discharge recorded at the Datong hydrologic station from 1950 to 2016 (Changjiang Water Resources Commission) was used in the model as the river boundary condition. Wind data, with

a resolution of 0.25°×0.25°, were adopted based on the semi-monthly mean of 10 years (2007-2017) from the NCEP (National Centers for Environmental Prediction) with a resolution of 0.25°×0.25° (https://www.ncep.noaa.gov).

For this study, two numerical experiments were conducted using the topographies measured in 2007 and 2017. However, the topography change trends of the past decade showed that the North Branch was heavily deposited and the channel became narrow (Fig.1 (a, b)). Therefore, an additional numerical experiment was conducted which made the North Branch complete silt-up on the basis of 2017 experiment. In this numerical experiment, the grids and topographies were same with the 2017 experiment but all wet grids in the North Branch were transformed into dry grids. Because the tide was just the oscillation of ocean waters under the influence of the attractive gravitational forces of the moon and the sun (Simm et al., 1996). So the differences of astronomical tides during dry season in different years were small. To make sure the tidal condition identical in three experiments, we selected the same simulation time. All model simulations covered the period from December 1, 2016 to February 28, 2017 which was the typical dry season. Because the model need 1-2 months to adjust the hydrodynamic and salinity to be stable. Therefore the model results in February were used to analyze and compare the impacts of the topography change over the past decade and the North Branch complete silt-up on residual water and salt transport, WDR, and saltwater intrusion. The monthly averaged river discharge since 1950 was 13600 m^3/s, 11100 m^3/s and 12000 m^3/s in December, January and February (dry season), and 36000 m^3/s, 45000 m^3/s and 40000 m^3/s in June, July and August (flood season), respectively. The river discharge in dry season is much lower than in flood season. The integrated time step was set to 30 s for all test cases.

To describe the water and salt transport, the residual unit width water flux (RUWF) and the

residual unit width salt flux (RUSF) are defined as follows.

$$\vec{Q} = \int_{h1}^{h2} \vec{V} d\sigma \tag{1}$$

$$RUWF = \frac{1}{T}\int_0^T \vec{Q} dt \tag{2}$$

$$RUSF = \frac{1}{T}\int_0^T \vec{Q} s dt \tag{3}$$

where $\vec{Q}$ is the instantaneous rate of water transport per unit width through a water column, $\vec{V}$ is the current vector, *h1, h2* is the lower and upper bound depth of a layer , and σ is the depth of layer bound. *T* is the time period (which equals one or several tidal cycles; in this study, it equals six semidiurnal tidal cycles) and is used as an averaging time window to remove the tidal signals, and *s* is salinity.

Additionally, the residual transection water flux (NTWF) is determined to calculate the WDR between channels (transection locations labeled in Fig. 1) as follows.

$$NTWF = \frac{1}{T}\int_0^T \int_{-H(x,y)}^{\zeta} \int_0^L \vec{V}_n(x,y,z,t) dl dz dt \tag{4}$$

where *T* is the same as above, ζ is the elevation, L *l* is the width of the transect, and $\vec{V}_n(x,y,z,t)$ is the velocity component that is vertical to the transect.

Similarly, the residual (net) transection salt flux (NTSF) is determined as follows.

$$NTSF = \frac{1}{T}\int_0^T \int_{-H(x,y)}^{\zeta} \int_0^L s\vec{V}_n(x,y,z,t) dl dz dt \tag{5}$$

where s is salinity.

2.3 Model Validation

The model has been extensively calibrated, validated and applied in a number of previous studies in the Changjiang Estuary, which have shown that the model can reproduce the

observed water level, current and salinity with high simulation accuracy (Li et al. 2012; Lyu and Zhu, 2018b; Qiu, et al., 2015; Wu and Zhu 2010). In this study, we used the measured data taken in the South Passage from 9th to 19th March 2018 (three ship sites and three buoy sites shown in Fig. 1b) to further validate the model results.

The river discharge at the Datong Hydrological Station and wind data recorded by the weather station located on the east of the Chongming Island (indicate by W in Fig. 1) were adopted during the measured period to run the model. Three skill assessment indicators were used to quantify the current and salinity validation: the correlation coefficient (CC), root mean square error (RMSE), and skill score (SS). As follows,

$$CC = \frac{\sum (X_{\mathrm{mod}} - \overline{X}_{\mathrm{mod}})(X_{obs} - \overline{X}_{obs})}{[\sum (X_{\mathrm{mod}} - \overline{X}_{\mathrm{mod}})^2 \sum (X_{obs} - \overline{X}_{obs})^2]^{1/2}} \tag{6}$$

$$RMSE = \sqrt{\frac{\sum (X_{\mathrm{mod}} - X_{obs})^2}{N}} \tag{7}$$

$$SS = 1 - \frac{\sum | X_{\mathrm{mod}} - X_{obs} |^2}{\sum (| X_{\mathrm{mod}} - \overline{X}_{obs} | + | X_{obs} - \overline{X}_{obs} |)^2} \tag{8}$$

where X_{mod} is the modeled data, X_{obs} is the observed data, and $\overline{X}$ is the mean value. SS is a statistical metric developed by Wilmott (1981) to describe the degree to which the observed deviations from the observed mean correspond to the predicted derivations from the observed mean. Perfect agreement between the model results and observations yields an SS of 1.0, whereas complete disagreement yields a value of 0. Temporal variations in the observed and modeled water velocities and salinities at ship-measured site B in the middle tide after neap tide and buoy-measured Buoy 2 were selected and shown in Fig. 3 and 4, respectively.

The assessment indicator scores of water velocity were summarized in Table 2. The values of CC at the six sites ranged from 0.63 to 0.93 in the surface layer and from 0.51 to 0.84 in the bottom layer; the RMSE ranged from 0.23 to 0.35 cm/s in the surface layer and from 0.10 to

0.21 m/s in the bottom layer; and the SS ranged from 0.79 to 0.93 in the surface layer and from 0.71 to 0.90 in the bottom layer. The mean water velocity values of CC, RMSE and SS at the surface and bottom layers at six sites were 0.77, 0.23 cm/s and 0.86, respectively.

The assessment indicator salinity scores were summarized in Table 3. The CC at the six sites ranged from 0.71 to 0.92 in the surface layer and from 0.66 to 0.90 in the bottom layer; the RMSE ranged from 0.36 to 2.49 in the surface layer and from 0.29 to 2.14 in the bottom layer; and the SS ranged from 0.80 to 0.96 in the surface layer and from 0.80 to 0.95 in the bottom layer. The mean salinity values of CC, RMSE and SS at the surface and bottom layers at the six sites were 0.83, 1.60 and 0.90, respectively. The assessment indicators indicated that the level of model performance reached a high standard.

Table 2

Values of CC, RMSE, and SS of the modeled and observed flow velocity at the surface and bottom layers at the measurement sites.

Layer	Sites	RMSE（m/s）	CC	SS
Surface	A	0.35	0.63	0.79
	B	0.23	0.93	0.89
	C	0.34	0.75	0.85
	Buoy 1	0.34	0.73	0.84
	Buoy 2	0.27	0.88	0.93
	Buoy 3	0.24	0.86	0.92
Bottom	A	0.21	0.51	0.71
	B	0.21	0.75	0.86
	C	0.18	0.73	0.84
	Buoy 1	0.11	0.78	0.87
	Buoy 2	0.12	0.84	0.90
	Buoy 3	0.10	0.80	0.88

Table 3

Values of CC, RMSE, and SS of the modeled and observed salinity at the surface and bottom layers at the measurement sites.

Layer	Sites	RMSE	CC	SS
Surface	A	1.88	0.73	0.85
	B	2.49	0.85	0.90
	C	2.24	0.71	0.80
	Buoy 1	2.33	0.87	0.93
	Buoy 2	1.73	0.92	0.96
	Buoy 3	0.36	0.83	0.89
Bottom	A	2.14	0.66	0.80
	B	1.57	0.92	0.95
	C	1.30	0.86	0.92
	Buoy 1	1.31	0.87	0.92
	Buoy 2	/	/	/
	Buoy 3	0.29	0.90	0.95

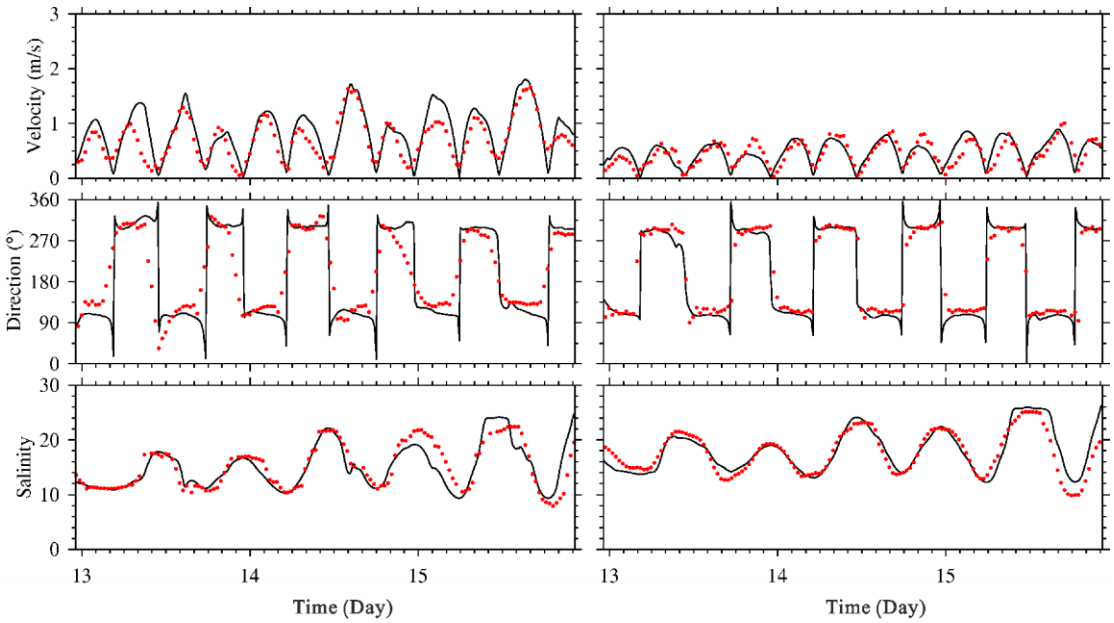

Fig. 3. Comparisons of modeled (line) and measured (dots) flow velocity/direction and salinity during neap tides at the surface layer (left panel) and bottom layer (right panel) at site B in March 2018.

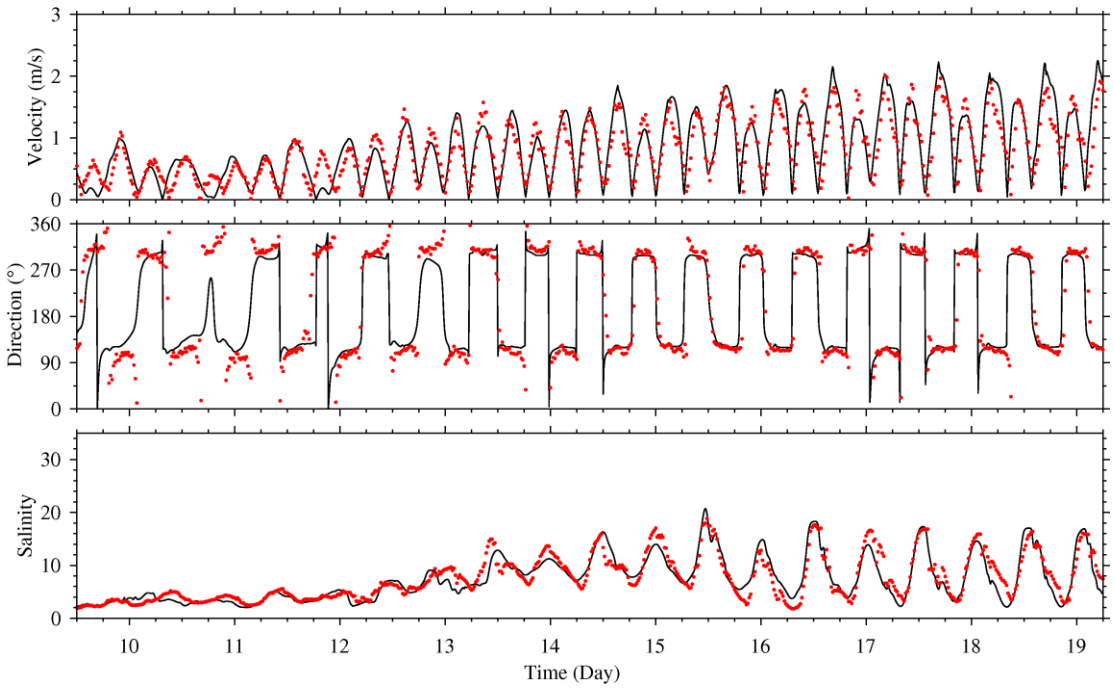

Fig. 4. Comparisons of modeled (line) and measured (dots) flow velocity/direction and salinity at the surface layer at site Buoy 2 in March 2018.

3. Results and Discussion

3.1 Topography change from 2007 to 2017

During the period from 2007 to 2017, some major reclamation projects were conducted in the Changjiang Estuary, including the reclamation projects in the Eastern Hengsha Shoal, the Qingcaosha Reservoir (shown in Fig. 1b) for the demands of land and water. These projects considerably changed the local topography and further changed the topography in the entire estuary by altering the hydrodynamic processes (Lyu and Zhu, 2018a; Zhu and Bao, 2016). Due to these anthropogenic activities, the Changjiang Estuary has undergone dramatic topography change from 2007 to 2017. Fig. 1 showed the estuarine topographies for 2007 and 2017, while the topography change in the recent decade was shown in Fig. 5. The topography was found markedly changed in some places. The topography in the lower reaches of the North Branch was deposited approximately by 2 - 4 m overall. The area in the lower reaches of the North Branch and near Chongming Island has turned into land from the tidal flat, which made it narrower and shallower. In the South Branch, the area south of Chongming Island silted severely, and the maximum value reached a thickness of 6 m, while the middle of the channel deepened. In the North Channel, the depth north of the middle and lower QCSR was heavily deposited. In contrast, the depth deepened greatly south of Chongming Island and north of the middle QCSR, in the middle of the channel and east end of the QCSR. Near the mouth of the North Channel, the depth silted overall except the area north of Hengsha Island. The area east of the reclamation project of Eastern Hengsha Shoal silted 2-4 m. In the South Channel, the depth in the upper reaches deepened by 2-4 m. The depth became shallow north of the North Passage and became deep in the main channel in a range of approximately 2 m. The depth variation in the South Passage was smaller compared with other channels in a range of approximately 1 m. And the net volume change in the North Branch, South Branch, North Channel, South Channel, North and South

Passages were -1.73×10^8, 3.24×10^8, 9.34×10^7, 2.90×10^8, -3.19×10^7 and 1.03×10^8 m^3, respectively (The negative indicates deposition). However, although the net volume changes in the North Channel indicated erosion as a whole, it was mainly eroded in the upper reaches. The lower reaches were significant deposition and net volume change in the lower reaches was -7.80 $\times10^7$ m^3.

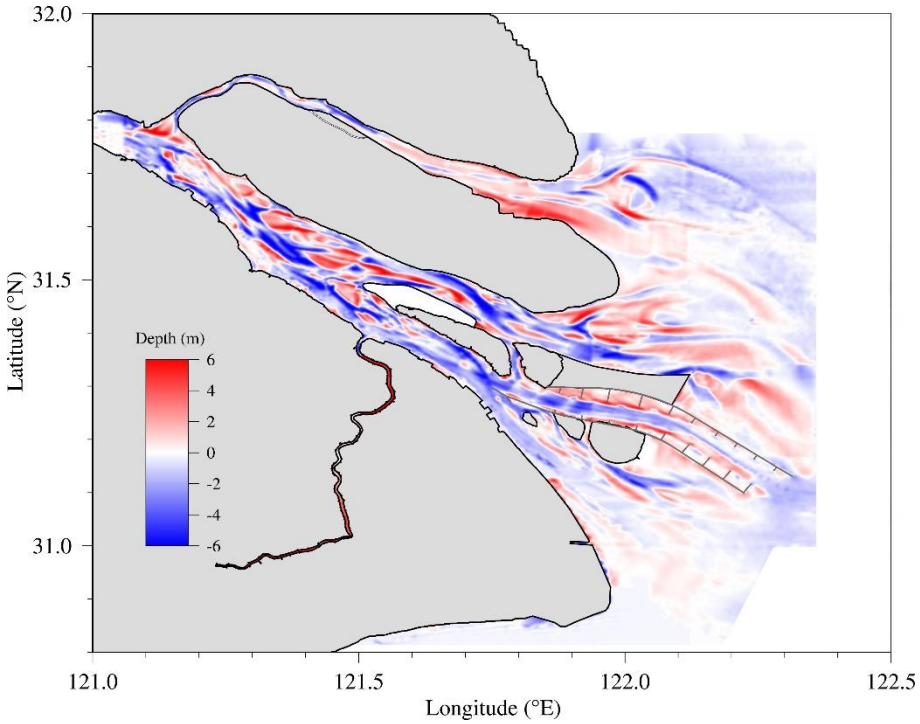

Fig. 5. Topographic changes between 2007 and 2017 indicated by water depth changes measured in 2007 in 2017 (-ve = deposition and +ve= erosion).

3.2 RUWF, RUSF, Saltwater Intrusion and WDR in 2007

Fig. 6a shows that the surface RUWF flowed seaward in the South Branch, North and South Passages during the spring tide, but the RUWF flowed into the estuary in the North Branch due to its funnel shape and tidal Stokes transport (Qiu and Zhu, 2015). This indicated that the river runoff flows into the sea mainly through the North Channel, North and South Passages. In the upper reaches of the North Branch, the NTWF and WDR were -300.1 m^3/s and

343 -2.6% (Table 4), respectively, where the negative sign indicated that the water was transported
344 from the North Branch into the South Branch. Most of the river runoff (72.8%) flowed into the
345 sea through the North Channel compared with the South Channel (Table 5). Similarly, the South
346 Passage was the main channel (54.3%) for the river runoff into the sea compared with the North
347 Passage (Table 6). The RUWF flowed northward east of Chongming Island due to tidal
348 pumping transport and tidal Stokes transport (Qiu and Zhu, 2015). Additionally, the RUWF in
349 the South Branch was seaward in both the surface and bottom layers but smaller in the bottom
350 layer due to bottom friction (Fig. 6b). Near the river mouth, the bottom RUWF was landward,
351 which was believed to be induced by a strong salinity front (Pritchard, 1956). The RUWF
352 flowed seaward in the surface layer and landward bottom layers east of the Eastern Hengsha
353 Shoal. As shown in Fig. 6(c, d), the distribution of RUSF was similar to that of RUWF. Due to
354 high salinity around the outside of the river mouth, the magnitude of the RUSF was much larger
355 in that area. On the northern side of the North Passage, the RUSF flowed landward, which
356 brought high salinity into the North Channel and the area east of Chongming Island. The North
357 Branch was occupied by the highly saline water, and the SSO was simulated, which was caused
358 by the RUWF and RUSF flowed into the South Branch from the North Branch in the upper
359 reaches (Fig. 6). The less saline water northeastward extended east of Chongming Island, which
360 corresponded to the RUSF. Obviously, the saltwater intrusion in the bottom was stronger.
361 Among each outlet in the Changjiang Estuary, the saltwater intrusion was the weakest in the
362 North Channel and strongest in the South Passage.

363 During neap tide (Fig. 7), around the area outside of the river mouth, the RUWF and RUSF
364 flowed southward because the northerly winter monsoon effect was dominant with the tide
365 becoming weaker (Wu et al., 2014). The SSO, which occurred during spring tide, disappeared.

The NTWF became positive (93 m^3/s), and the WDR was 0.7% (Table 4). Compared with the South Channel, the North Channel was the main channel for river discharge, which accounts for 66.7% (Table 5). Compared with the South Passage, more river runoff flowed into the sea from the North Passage, accounting for 86.6% (Table 6), which was due to blocking of the stronger salinity front in the South Passage. Near the river mouth, due to a strong horizontal salinity gradient, the RUWF and RUSF in the bottom layer flow landward obviously. The saltwater induced by the SSO during spring tide has arrived at the middle reaches of the South Branch. Because the tidal mixing become weaker in neap tide than in spring tide, there existed distinct saltwater wedges near the river mouth in neap tide, resulting in high stratification, i.e., the bottom salinity was greater than the surface salinity.

Table 4

NTWF and WDR in the North and South Branches (NB and SB) during spring and neap tides in 2007 and 2017

Year	NTWF (m^3/s)				WDR (%)			
	Spring		Neap		Spring		Neap	
	NB	SB	NB	SB	NB	SB	NB	SB
2007	-300.1	11804.9	93.4	12779.8	-2.6	102.6	0.7	99.3
2017	-330.9	11842.4	199.1	12606.8	-2.9	102.9	1.6	98.4
$\triangle_{2017-2007}$	-30.8	37.5	105.7	-173.0	-0.3	0.3	0.9	-0.9

Table 5

NTWF and WDR in the North and South Channels (NC and SC) during spring and neap tides in 2007 and 2017

Year	NTWF (m^3/s)				WDR (%)			
	Spring		Neap		Spring		Neap	
	NC	SC	NC	SC	NC	SC	NC	SC
2007	8507.7	3180.4	8631.3	4303.8	72.8	27.2	66.7	33.3
2017	7655.1	4055.0	8060.2	4630.7	65.4	34.6	63.5	36.5
$\triangle_{2017-2007}$	-852.6	874.6	-571.1	326.9	-7.4	7.4	-3.2	3.2

Table 6

NTWF and WDR in the North and South Passages (NP and SP) during spring and neap tides in 2007 and 2017.

Year	NTWF (m^3/s)				WDR (%)			
	Spring		Neap		Spring		Neap	
	NP	SP	NP	SP	NP	SP	NP	SP
2007	2707.3	2282.2	5266.3	817.1	54.3	45.7	86.6	13.4
2017	3460.5	1750.9	5132.7	818.7	66.4	33.6	86.2	13.8
$\triangle_{2017-2007}$	753.2	-531.3	-133.6	1.6	12.1	-12.1	-0.4	0.4

392 **Table 7**

393 NTSF in the North and South Branches (NB and SB) during spring and neap tides in 2007 and

394 2017

Year	NTSF (t/s)			
	Spring		Neap	
	NB	SB	NB	SB
2007	-7.70	7.45	0.03	0.12
2017	-6.10	5.81	0.04	0.12
$\triangle_{2017-2007}$	1.60	-1.64	0.01	0.00

395

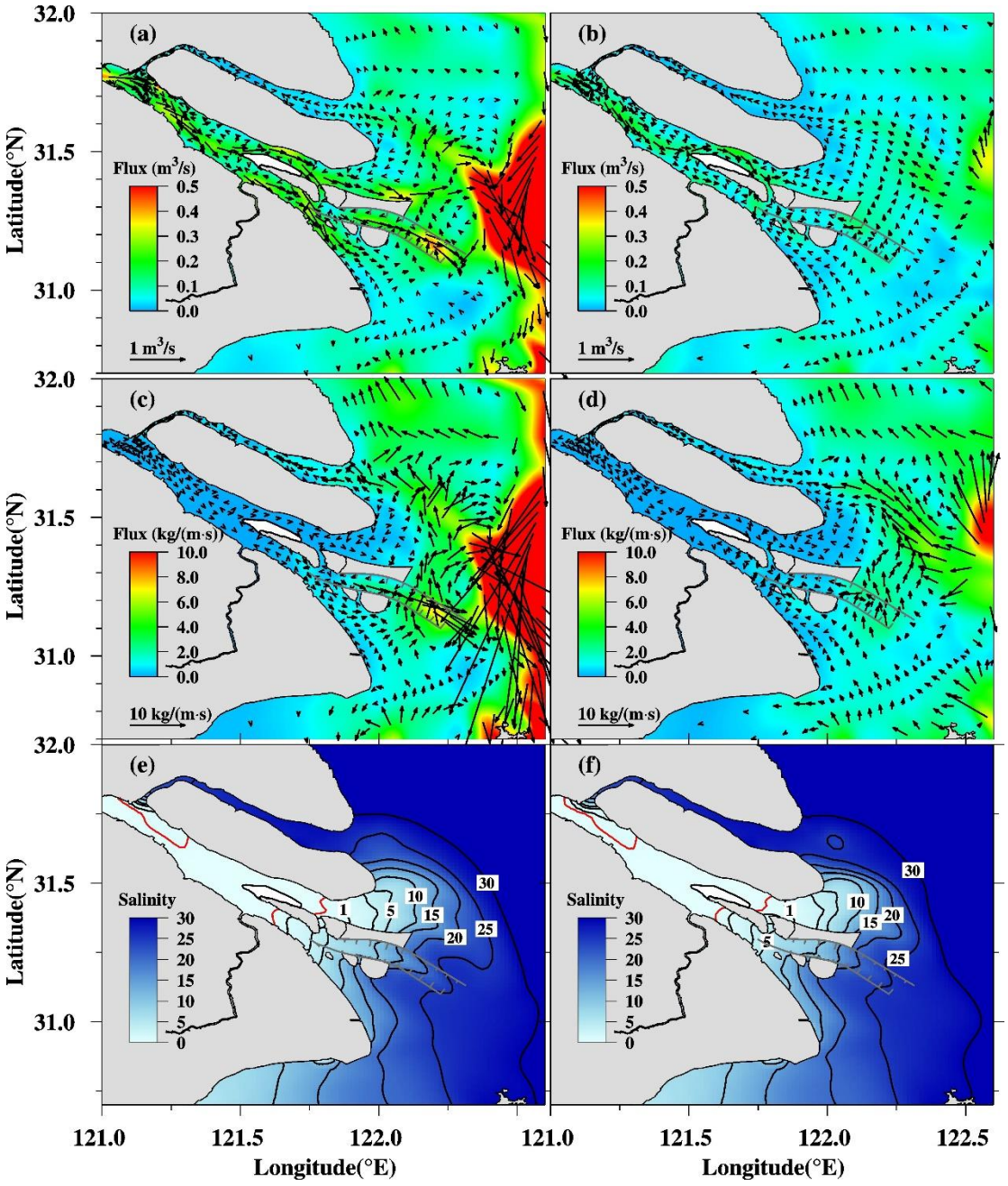

396

397 **Fig. 6.** Distributions of RUWF (a, b), RUSF (c, d) and salinity (e, f) in the surface (left panel)

398 and bottom (right panel) layers during spring tides in 2007. (The red isohalines in (e, f) are 0.45,

399 the standard salinity for drinking water).

400

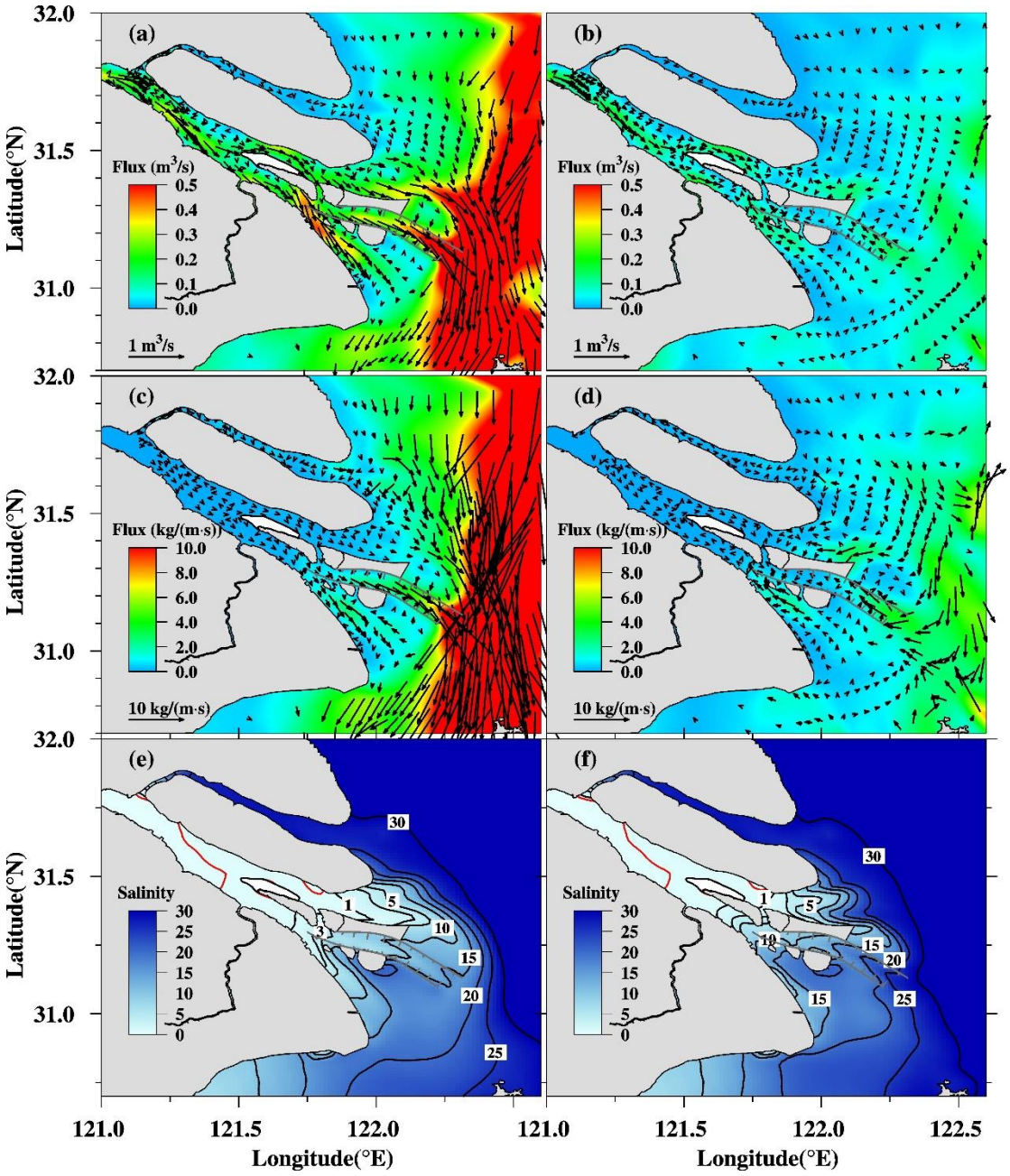

401

402 **Fig. 7.** Distributions of RUWF (a, b), RUSF (c, d) and salinity (e, f) in the surface (left panel)

403 and bottom (right panel) layers during neap tides in 2007.

404

405 **3.2 RUWF, RUSF, Saltwater Intrusion and WDR in 2017**

406 The differences in distributions of the RUWF, RUSF and salinity between 2017 and 2007

407 in the surface and bottom layers during spring tide were shown in Fig. 8. The differences of

408 RUWF and RUSF in the North Branch were landward, which was the same direction as RUWF

409 and RUSF in 2007, which meant that the saline transport from the sea to the North Branch
410 increased in 2017. However, the salinity in the North Branch decreased overall as shown in Fig.
411 8(e, f). This was because the topography became narrower and shallower in the middle and
412 lower reaches of the North Branch (as shown in Fig. 1 and Fig. 5), which resulted in a decrease
413 in the tidal volume. This could also cause the increase in the North Branch water velocity, so
414 that the RUWF and RUSF increased. The NTWF in the North Branch was -330.9 m^3/s, which
415 increased by 30.8 m^3/s from the North Branch to the South Branch, but the NTSF decreased 1.6
416 t/s (Table 7). Therefore, the SSO became weaker overall in 2017 than in 2007. The salinity in
417 the South Branch changed little. However, Fig.5 showed that major changes in topography were
418 detected along the Southern Branch. It can be seen from Fig. 6(e, f) and Fig. 7(e, f) that the
419 South Branch was almost occupied by freshwater because the South Branch is the main channel
420 for river water discharging into the sea. Therefore, though major changes in topography were
421 detected along the Southern Branch, the salinity was very low and its change was small.
422 However, the topography changes in the South Branch could influence the water diversion
423 ration in the North and South Branch, which could further influence the saltwater intrusion near
424 the river mouth where there existed salinity front. A small change of water diversion ration can
425 cause obvious isohaline move. That is why all the changes in isohaline were noticed near the
426 mouth and further seaward. The difference of RUWF and RUSF in the North Channel was
427 strongly correlated with that of the topography. The RUWF and RUSF increased with the
428 increase of water depth. Fig. 8(e, f) show that the salinity in the North Channel increased,
429 especially in the area east of Chongming Island and Eastern Hengsha Shoal, with a maximum
430 value of more than 4.0. The deposition in these areas was noticeable (Fig. 5), which blocked the
431 freshwater discharge into the North Channel. The WDR in the North Channel was 65.4% in

2017, which decreased by 7.4% compared with 2007 (Table 5), resulting in an overall increase in salinity in the North Channel in 2017. Owing to the decrease in lower salinity water that flowed over the area east of the Eastern Hengsha Shoal, the amount of lower saline water that flowed cross the north dyke of the Deep Waterway to the south decreased under the action of the north winter monsoon. Therefore, the salinity near the mouth of the North and South Passages slightly increased.

During neap tide, the patterns of difference in the distributions of the RUWF, RUSF and salinity between 2007 and 2017 in the surface and bottom layer were different from those during spring tide, and the variations were the opposite in some areas (Fig. 9). In the North Branch, the RUWF and RUSF showed little change with the weaker tide, while the WDR increased in 2017, which caused the salinity in the North Branch to decrease overall. In the South Branch, the difference in RUWF and RUSF was correlated with the difference in the topography. Similar to that in the spring tide, the salinity east of Chongming Island and Eastern Hengsha Shoal increased. However, the surface salinity near the 122.5°E area in the mouth of the North Channel and the bottom salinity north of the Eastern Hengsha Shoal decreased by more than 4.0 at its maximum. As shown in Fig. 9, the difference in the surface RUSF (Fig. 9c) was the opposite of the surface RUSF (Fig. 7c) in 2007 near the 122.5°E area in the mouth of the North Channel. This meant that the high salinity water from the north decreased. The bottom salinity decreased because the saltwater wedge weakened. The salinity variation, s', at each layer and its mean value in the water column can be estimated with a polynomial expression given by Hansen and Rattray (1966),

$$s' = \frac{H^2}{K_S}\overline{s}_x\left[\overline{u}\left(-\frac{7}{120}+\frac{1}{4}\zeta^2+\frac{1}{4}\zeta^2-\frac{1}{8}\zeta^4\right)+u_E\left(-\frac{1}{12}+\frac{1}{2}\zeta^2-\frac{3}{4}\zeta^4-\frac{2}{5}\zeta^5\right)\right] \quad (6)$$

where s indicates the width-averaged, tidally averaged salinity, which can be divided into depth-average ($\overline{s}$) and depth-varying (s') parts. The subscript x denotes the along-channel partial derivative. K_S is the vertical eddy diffusivity; the dimensionless coordinate $\zeta = z/H$, where z indicates water depth, with $z=0$ as the surface layer and $z=-H$ as the bottom layer, and H indicates topography. River discharge is given by $\overline{u}$, $u_E = g\beta\overline{s}_x H^3/(48K_M)$, where $\beta \cong 7.7\times10^{-4}/PSU$ and K_M indicates the vertical eddy viscosity. When $z=0$ and $z=-H$, formula (6) can be written as follows:

$$\begin{cases} s' = -\dfrac{H^2}{120K_S}\overline{s}_x(7\overline{u}+10u_E) & z=0 \\ s' = \dfrac{H^2}{15K_S}\overline{s}_x(\overline{u}+u_E) & z=-H \end{cases} \tag{7}$$

It is clear that the increased H can augment the salinity variation s'. Therefore, as the depth near the mouth of the North Channel was deposited all together (as shown in Fig. 5), the decreased H reduced the variation s' near the bottom, resulting in a weaker gravitational circulation that transported less oceanic saltwater into the estuary and decreased the bottom salinity. Additionally, although the WDR in the North and South Passages had little variation, namely, approximately 0.4%, the WDR in the South Channel increased by 3.2% in 2017, resulting in a slight decrease in salinity.

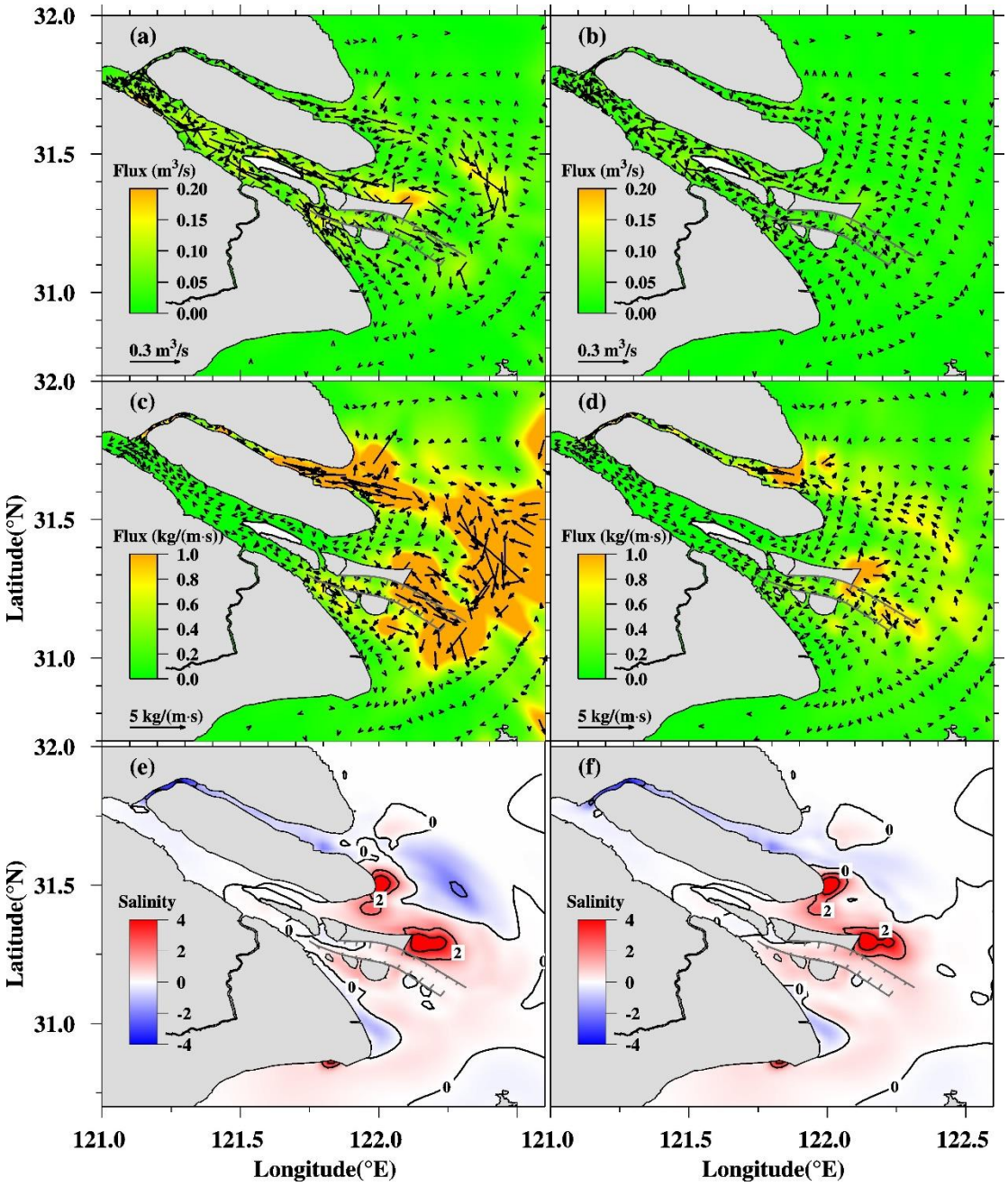

Fig. 8. Changes of RUWF (a, b), RUSF (c, d) and salinity (e, f) between 2017 and 2007 in the surface (left panel) and bottom (right panel) layers during spring tides.

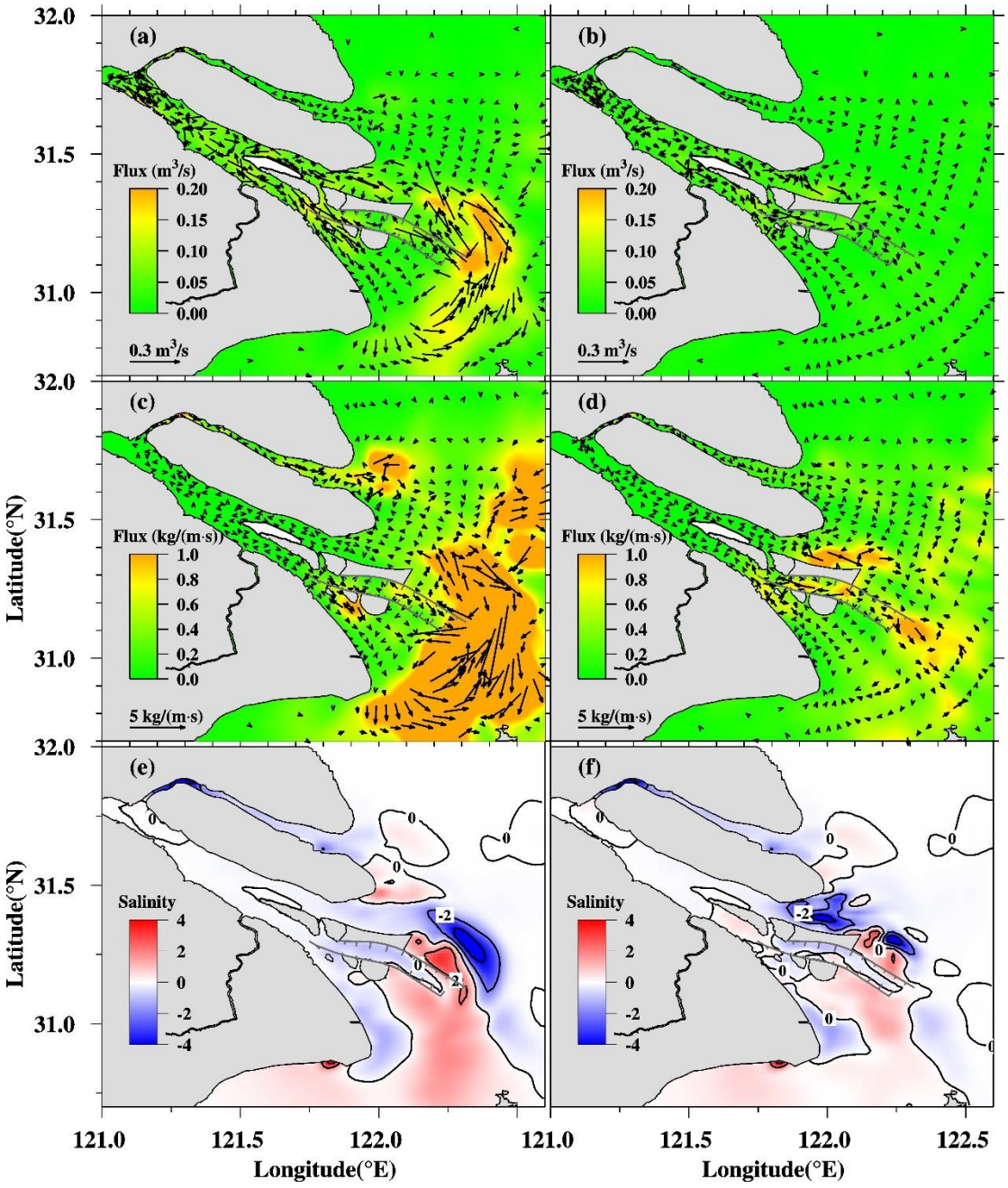

474

475 **Fig. 9.** Changes of RUWF (a, b), RUSF (c, d) and salinity (e, f) between 2017 and 2007 in the

476 surface (left panel) and bottom (right panel) layers during neap tides

477

478 **3.3 Variations in Vertical Salinity Distributions**

479 The vertical distributions of salinity during spring tide along the North Branch profile (P1),

480 South Branch-North Channel profile (P2) and South Branch-South Passage profile (P3) in 2007

481 and 2017 are shown in Fig. 10. It was obvious that the depth near the bifurcation of the North

and South Branches became shallower. The depth at the start point of P1 was approximately 7.2 m in 2007, but it became approximately 0.3 m in 2017. Although the depth at nearly 17.5 km increased from 11.5 to 15.2 m over the ten year period, the average depth from 40 to 80 km decreased from 7.3 to 6.62 m. Therefore, it would certainly decrease the tidal volume in the North Branch. In Fig. 10a, the isohaline was densely distributed between 0 and 20 km, and the bottom salinity was higher than the surface salinity. The isohaline distribution was sparser in 2017, and the isohaline of 20 moved downstream from 10 km to 20 km. Overall, the saltwater intrusion in the North Branch became weaker in 2017 than in 2007. The vertical salinity distributions along P2 in 2007 and 2017 are shown in Fig. 10b. The water depth in 2017 became shallow overall. In the upstream and midstream areas, the depth changed slightly, except for the area near 7 km, which decreased from 52.4 to 35.4 m. The average depth in the downstream, namely, from 80 km to the end of P2, decreased from 9.9 to 9.1 m. The salinity in the upstream region was less than 0.45, indicating that freshwater existed. The intensity of SSO weakened in 2017, which could be proven by the location of the bottom isohaline being 1 in 2007. Nearly all the isohalines in the downstream moved upstream by approximately 5 km in 2017 compared to 2007. Therefore, the saltwater intrusion along the North Channel was enhanced in 2017. The vertical salinity distributions along P3 in 2007 and 2017 are shown in Fig. 10(e, f). The variation in depth was great at a distance of approximately 5 km from the start point of P3, which decreased from 53.9 to 41.8 m. Compared with the isohaline distribution in 2007, the variation was very small. In 2017, the isohalines moved upstream by approximately 1 km compared with that in 2007. The saltwater intrusion increased slightly in 2017.

During neap tide, the salinity upstream of the North Branch decreased markedly. In 2007, isohaline 0.45 appeared (Fig. 11a). Similar to that in the spring tide, the isohalines moved

downstream by approximately 5 km in 2017. The saltwater intrusion in the North Branch was also weakened in 2017. However, unlike during spring tide, the saltwater intrusion in the North Channel became weaker in 2017 than that in 2007 because the main character of the saltwater intrusion during neap tide was a salt wedge (Fig. 11b). Fig. 10c shows that the bottom salinity was much greater than the surface salinity regardless of being in the North Channel or South Passage. The average depth downstream was decreased from 9.9 m in 2007 to 9.1 m in 2017, resulting in a reduction in bottom salinity. Isohaline 1 moved downstream by approximately 8 km in 2017, and isohaline 5 retreated from 82 km in 2007 to 88 km in 2017. Relative to the North Channel, the depth in the South Passage showed little change. Because the WDR in the South Channel increased from 33.3% to 36.5% over the last ten years, the saltwater intrusion was weakened in 2017.

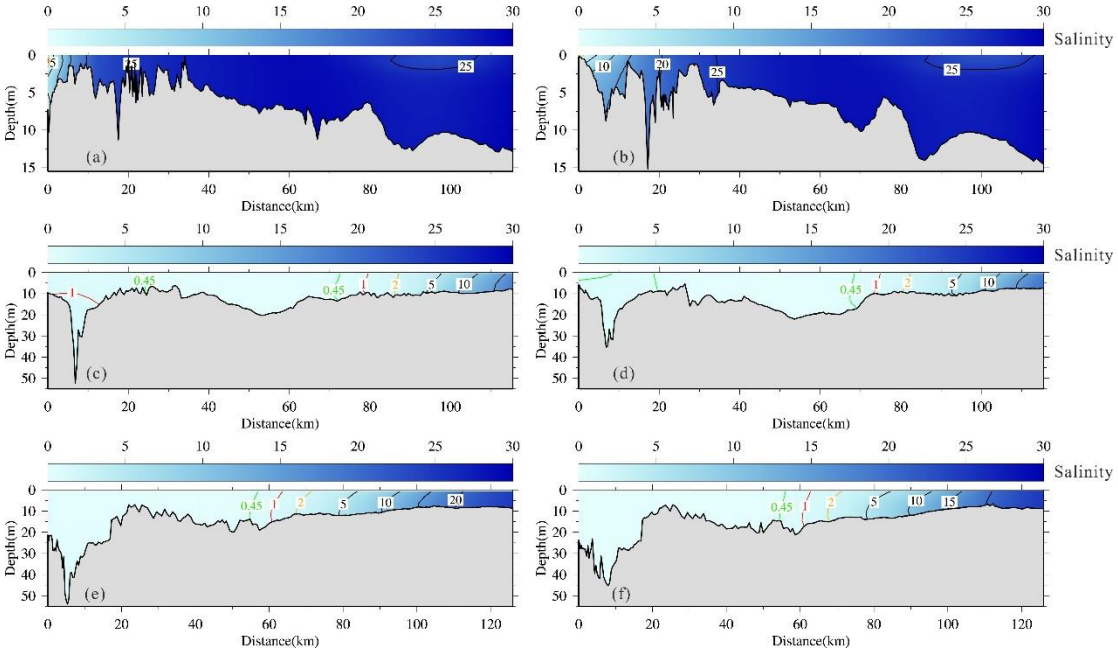

Fig. 10. Distribution of salinity along profiles P1(a, b), P2 (c, d) and P3 (e, f) during spring tides in 2007 (left panel) and 2017 (right panel)

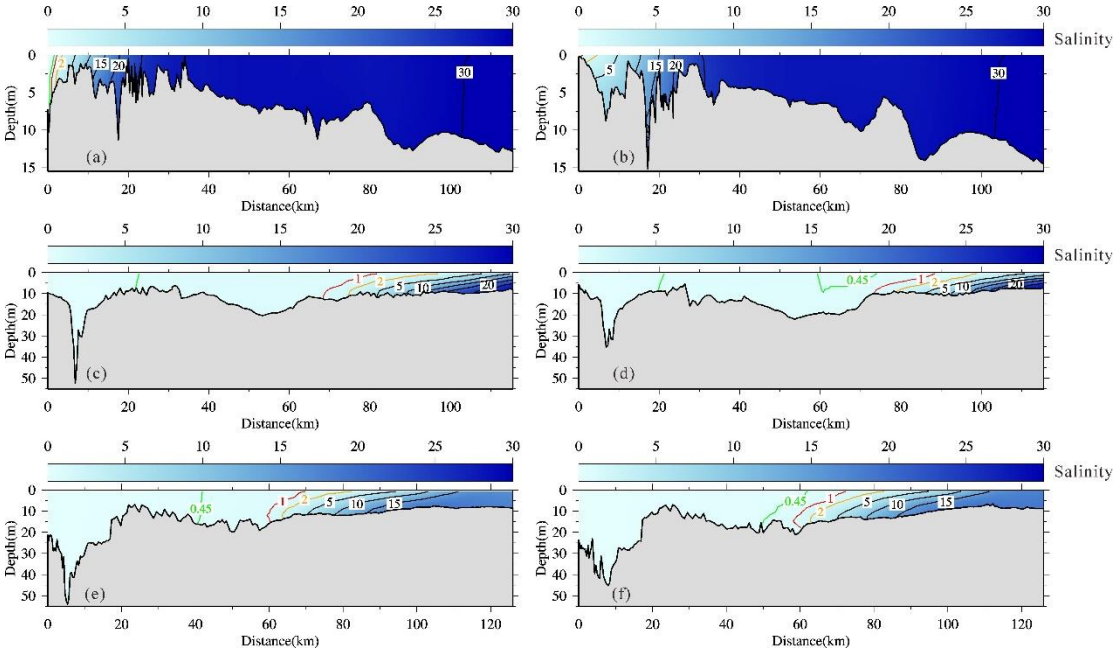

Fig. 11. Distribution of salinity along profiles P1(a, b), P2 (c, d) and P3 (e, f) during neap tides in 2007 (left panel) and 2017 (right panel)

3.4 Scenario of Complete Silt-up of the North Branch

Over hundred years ago, the North Branch was the main channel discharging the river water into the sea and sediments were gradually deposited, especially since the 1960s, due to large tidal flat reclamation (Shen et al., 2003). Comparing the topography change in 2017 and 2007, the deposition at the upper entrance of the North Branch was very severe (Fig. 5). It is generally acknowledged that the North Branch will completely silt-up in the future. So we suppose the scenario that the North Branch would vanish and simulate its impact on saltwater intrusion and freshwater resources.

The SSO disappeared in the scenario of the North Branch silt-up, resulting in a salinity decrease in the South Branch. On the other hand, the river discharge was reduced in the North Channel, North and South Passages because there was no water spillover from the North Branch into the South Branch, which accounted for 2.9% of the total river discharge during the

spring tide in 2017 (Table 3), resulting in enhanced saltwater intrusion (Fig. 12). The salinity decrease was at the upper reaches of the South Branch during spring tide and moved down to the middle and lower reaches of the South Branch. Salinities at the water intakes of the three reservoirs all decreased. The maximum salinity increase east of Chongming Island reached 2. Therefore, vanishing of the North Branch weakened the saltwater intrusion in the South Branch and enhanced it in the North Channel, North and South Passages.

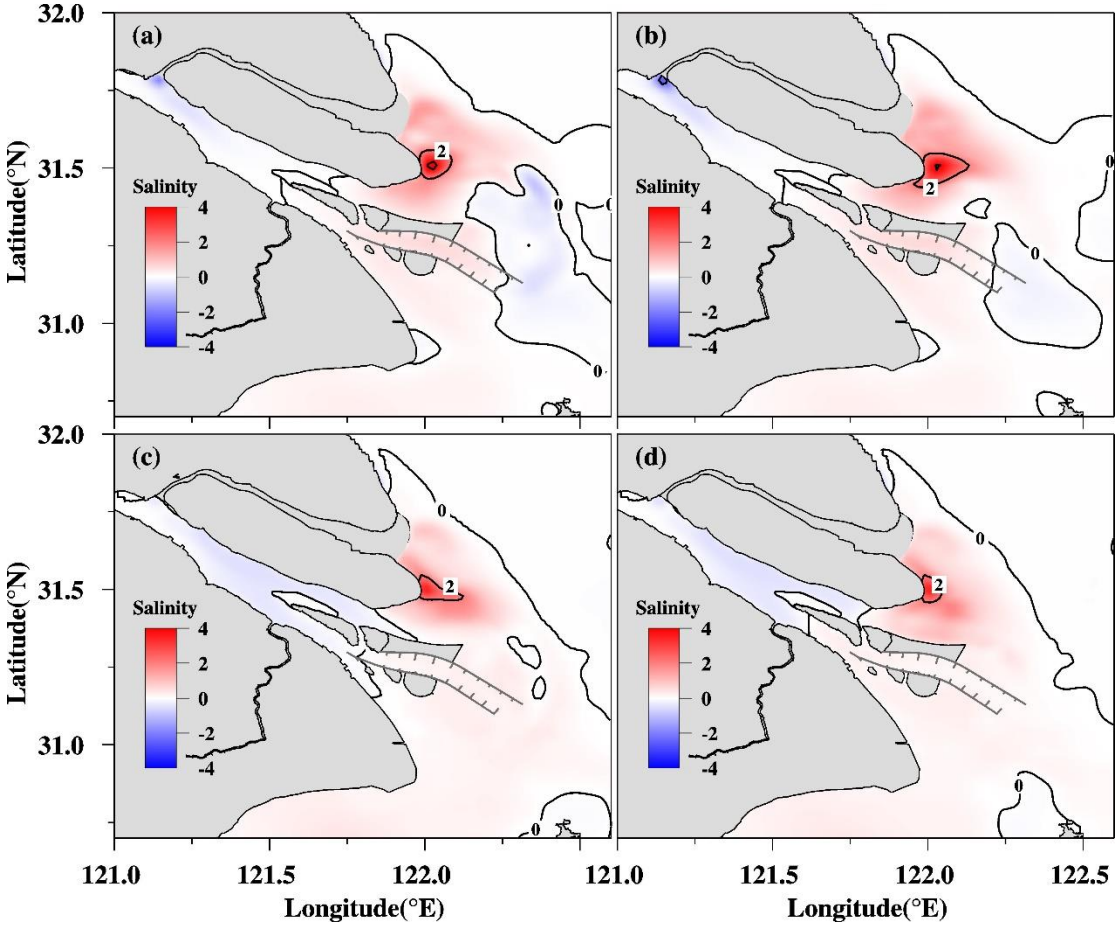

Fig. 12. Changes in salinity between the scenario of complete silt-up in the North Branch and 2017 topography in the surface (left panel) and bottom (right panel) layers during spring tides (a, b) and neap tide (c, d).

3.5 Impacts on Water Resources

548 The saltwater intrusion frequently threatens the freshwater intake from the Changjiang
549 Estuary during winter due to low river discharge. Confirming the results of past studies, the
550 salinities at the DFXSR and CHR were completely influenced by the SSO, but the QCSR was
551 mainly impacted by the SSO and the saltwater intrusion along the North Channel (Chen and
552 Zhu, 2014; Li and Zhu, 2018; Lyu and Zhu, 2018b).

553 The temporal surface salinity variations and tidally averaged salinity in different tidal
554 patterns (spring, middle tide after the spring tide (MTST), neap and middle tide after the neap
555 tide (MTNT)) at the water intakes of the DFXSR, CHR and QCSR in 2007, in 2017 and in the
556 scenario of vanishing of the North Branch are shown in Fig. 13 and Table 8, respectively. The
557 temporal variations in the salinities showed that there were semidiurnal flood and ebb periods
558 and semimonthly spring and neap period variations induced by tide. In 2007 and 2017, at the
559 water intake of the DFXSR, the salinity was higher during the spring and MTST, and the
560 salinity was lower during the neap and MTNT. The duration in which the salinity was lower
561 than 0.45 was approximately half of the time in 2007 and 2017 in a complete neap-spring cycle,
562 and the reservoir had enough time to take water from the Changjiang Estuary. In 2007, the
563 tidally averaged salinity at the water intake of the DFXSR during spring tide, MTST, neap tide
564 and MTNT were 0.80, 0.97, 0.16 and 0.08, respectively. At the water intake of the CHR, the
565 duration in which the salinity was lower than 0.45, was greater than two-thirds of the time.
566 Additionally, it took approximately 2.0 days for the saline water induced from the SSO flowed
567 downstream to move from the water intake of the DFXSR to the water intake of the CHR,
568 which we determined by comparing the salinity peak phase difference at the water intakes of
569 the CHR and DFXSR (Fig. 13). In 2007, the tidally averaged salinity at the water intake of
570 CHR during spring tide, MTST, neap tide and MTNT were 0.09, 0.74, 0.31 and 0.02,

571 respectively, meaning that water resources were optimistic in the CHR except during MTST. In
572 2007, at the water intake of the QCSR, the duration in which the salinity was lower than 0.45
573 was approximately half of the time. The tidally averaged salinity at the water intake of the CHR
574 during spring tide, MTST, neap tide and MTNT were 0.10, 0.50, 0.53 and 0.22, respectively,
575 meaning that water resources were optimistic in the QCSR except during MTST and neap tide.
576 The above simulated temporal variation processes in salinity at the water intakes of three
577 reservoirs were reasonably close to the published studies (Zhu et al., 2013; Zhu and Wu, 2013;
578 Chen et al., 2019).

579 As mentioned above, the SSO were somewhat weakened after the last ten years, which
580 resulted in the salinity being slightly decreased overall at the water intakes of the DFXSR, CHR
581 and QCSR (Fig. 13). Owing to the saltwater sources were mainly from the SSO, the salinity
582 was decreased by 0.17 and 0.06 at the water intake of the DFXSR during spring tide and MTST,
583 and there were no changes during neap tide or MTNT. The salinity was decreased by 0.07 and
584 0.16 at the water intake of the CHR during spring tide and MTST, and there was a slight
585 increase of 0.02 during MTNT. The salinity decreased by 0.00, 0.09, 0.04 and 0.02 at the water
586 intakes of the QCSR during spring tide, MTST, neap tide, and MTNT, respectively, which
587 meant that the change in topography in the past ten years was favorable for the water resources
588 of the three reservoirs in the Changjiang Estuary.

589 In the scenario of vanishing of the North Branch, the salinity approached 0 at the water
590 intakes of the DFXSR and CHR and significantly decreased at the water intake of the QCSR
591 due to vanishing of the SSO. The scenario of complete silt-up in the North Branch was greatly
592 favorable for the utilization of freshwater resources in the Changjiang Estuary.

593

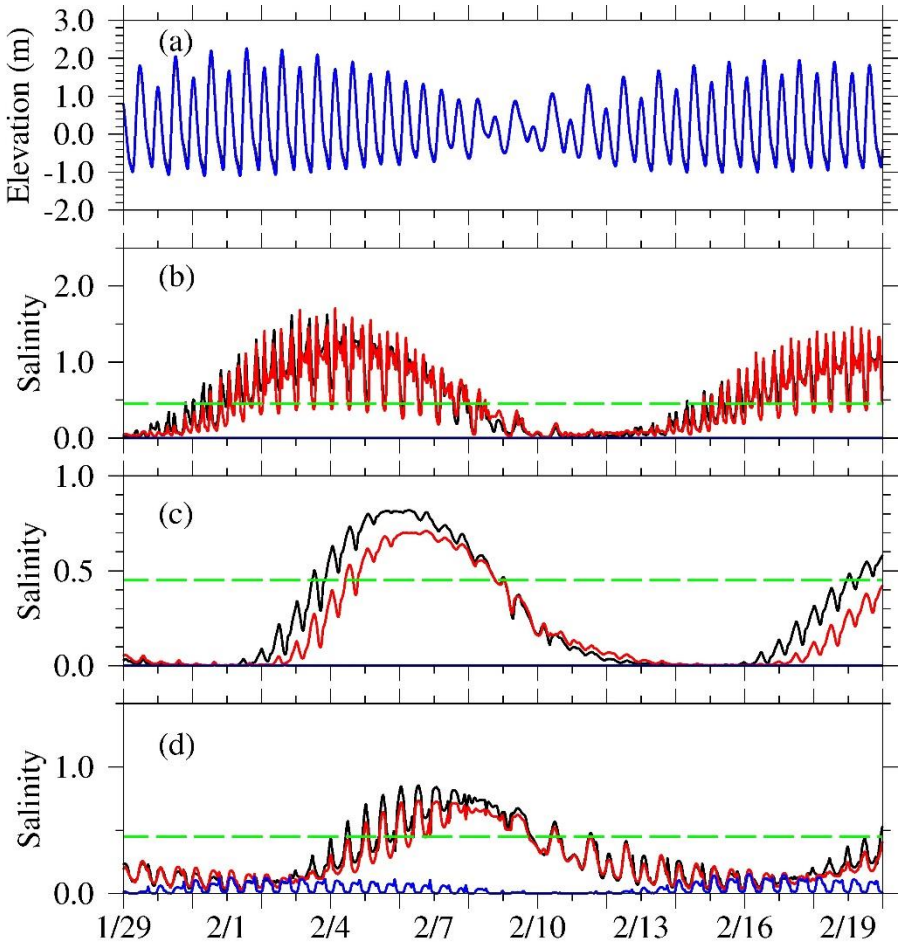

Fig. 13. Time series of computed water levels at the water intake of the QCSR (a), surface salinity at the water intakes of the DFXSR (b), CHR (c) and QCSR (d) from January 29 to February 19. (Black lines: 2007 topography; red lines: 2017 topography; blue line: complete silt-up in the North Branch; green dashed line: the standard salinity of drinking water).

Table 8

Averaged salinity over four tidal patterns at the water intakes of the DFXSR, CHR and QCSR in 2007 and 2017, the scenario of complete silt-up in the North Branch and in 2017

		Spring	MTST	Neap	MTNT
DFXSR	2007	0.80	0.97	0.16	0.08
	2017	0.63	0.91	0.16	0.08

	Scenario	0.00	0.00	0.00	0.00
	$\triangle_{2017\text{-}2007}$	-0.17	-0.06	0.00	0.00
	$\triangle_{scenario\text{-}2017}$	-0.63	-0.91	-0.16	-0.08
CHR	2007	0.09	0.74	0.31	0.02
	2017	0.02	0.58	0.31	0.04
	Scenario	0.00	0.00	0.00	0.00
	$\triangle_{2017\text{-}2007}$	-0.07	-0.16	0.00	0.02
	$\triangle_{scenario\text{-}2017}$	-0.02	-0.58	-0.31	-0.04
QCSR	2007	0.10	0.50	0.53	0.22
	2017	0.10	0.41	0.49	0.20
	Scenario	0.06	0.05	0.01	0.02
	$\triangle_{2017\text{-}2007}$	0.00	-0.09	-0.04	-0.02
	$\triangle_{scenario\text{-}2017}$	-0.04	-0.36	-0.48	-0.18

4. Conclusions

A well-validated 3D numerical model was used to simulate the impacts of topography change on saltwater intrusion over the past decade in the Changjiang Estuary. The residual water and salt transport, WDR and water resources with the topographies measured in 2007 and 2017 in the Changjiang Estuary were analyzed. During the period from 2007 to 2017, the reclamation projects and the changing climate resulted in a considerable change in topography in the estuary. The model was validated with the data measured in the South Passage in March 2018 and the results showed that the model produced satisfactorily the hydrodynamics and saltwater intrusion in the Changjiang Estuary.

The RUWF, RUSF, WDR and salinity distribution in 2007 and 2017 and the impacts of topography change in the last ten years were simulated and analyzed. Due to the topography change in the past ten years, the salinity decreased overall regardless of spring tide or neap tide in the North Branch, which was caused by the much shallower and narrower channel, resulting in a weaker SSO. In the North Channel, the salinity increased during spring tide, and the saltwater wedge weakened during neap tide due to a decrease in depth near the river mouth. The salinity increased slightly near the mouth of the North and South Passages during spring tide and decreased slightly in the upper reaches of the North and South Passages during neap tide. The changes in the saltwater intrusions in each channel were dynamically interpreted with the changes in RUWF, RUSF and WDR.

For the three reservoirs, there was about half time in a spring-neap period to take freshwater from the Changjiang Estuary into the reservoirs in the dry season of 2007 and 2017 under mean river discharge. Because the saltwater intrusion in the North Branch and the SSO were weakened over the last ten years, the salinity at the water intakes of the DFXSR, CHR and QCSR decreased slightly, which was favorable for the fresh resources of the three reservoirs in the Changjiang Estuary.

In the scenario of complete silt-up in the North Branch, the SSO disappeared, and saltwater weakened in the South Branch, which was significantly favorable for the utilization of freshwater resources and enhances the North Channel, North and South Passages.

On the whole, influenced by the topography change in recent decade, saltwater intrusion weakened in the North Branch, enhanced in the North Channel, North and South Passages during spring tide and weakened during neap tide. Moreover, the results showed that the deposition or even complete silt-up in the North Branch was favorable for utilization of freshwater resources.

Acknowledgements

This work was partly supported by the National Natural Science Foundation of China (41676083), Shanghai Institute of Eco-Chongming and China Scholarship Council (CSC). The insightful suggestions from the anonymous reviewers are also acknowledged.

Appendix 1: A list of acronyms and their corresponding full names in the paper

Acronym	Full Name
SSO	Saltwater spillover
DFXSR	Dongfengxisha Reservoir
CHR	Chenhang Reservoir
QCSR	Qingcaosha Reservoir
NCEP	National Centers for Environmental Prediction
RUWF	Residual unit width water flux
RUSF	Residual unit width salt flux
NTSF	Net transection salt flux
NTWF	Net transection water flux
WDR	Water diversion ratio
CC	Correlation coefficient
RMSE	Root mean square error
SS	Skill score
MTNT	Middle tide after the neap tide
MTST	Middle tide after the spring tide

643 **References**

644 Blumberg, A.F., 1994. A primer for ECOM-si. Technical report of HydroQual, 66.

645 Chen, C.S., Zhu, J.R., Ralph, E., Green, S.A., Budd, J.W., Zhang, F.Y., 2001. Prognostic
646 modeling studies of the Keweenaw current in Lake Superior. Part I: Formation and
647 evolution. Journal of Physical Oceanography, 31 (2), 379-395.
648 https://dx.doi.org/10.1175/1520-0485(2001)031<0379:PMSOTK>2.0.CO;2.

649 Chen, C.S., Zhu, J.R., Zheng, L.Y., Ralph, E., Budd, J.W., 2004. A non-orthogonal primitive
650 equation coastal ocean circulation model: application to Lake Superior. Journal of Great
651 Lakes Research, 30, 41-54. https://doi.org/10.1016/S0380-1330(04)70376-7.

652 Chen, J., Zhu, J.R., 2014a. Impact of the reclamation project of Xincunsha on the saltwater
653 intrusion in the North Branch of the Changjiang Estuary. Journal of East China Normal
654 University (Natural Science), 4, 163-172. [in Chinese with English abstract].

655 Chen, J., Zhu, J.R., 2014b. Sources for saltwater intrusion at the water intake of Qingcaosha
656 Reservoir in the Changjiang Estuary. Acta Oceanologica Sinica, 36, 131-141.

657 Chen, Q., Zhu, J.R., Lyu. H.H., Chen, S.L., 2019. Determining Critical River Discharge as a
658 Means to Provide Water Supply Security to the Changjiang River Estuary, China. Journal
659 of Coastal Research, published online.
660 https://www.jcronline.org/doi/abs/10.2112/JCOASTRES-D-18-00165.1

661 Geyer, W. R., 1993. The importance of suppression of turbulence by stratification on the
662 estuarine turbidity maximum. Estuaries and Coasts,16(1), 113-125.
663 https://dx.doi.org/10.2307/1352769.

664 Hansen, D.V., Rattray J.M., 1966. Gravitational circulation in straits and estuaries. Technical
665 Report No. 188, Department of Oceanography, University of Washington, Seattle,

Washington.

Ippen, A.T., 1966. Estuary and Coastline Hydrodynamics. McGraw-Hill, New York, NY, USA, ISBN 978 00 7032 015 4, p.744.

Ippen, A.T., Harleman, D.R.F., 1961. One-dimensional analysis of salinity intrusion in estuaries.Technical Bulletin no. 5, Committee on Tidal Hydraulics Waterways Experiment Station, Vicksburg, Mississippi.

Kantha, L.H., Clayson, C.A., 1994. An improved mixed layer model for geophysical applications. Journal of Geophysical Research Oceans, 99 (C12), 25235–25266. https://dx.doi.org/10.1029/94JC02257.

Li, G.P., Zhu, J.R., 2018. Analyses of saltwater intrusion at the water intake of qingcaosha reservoir in the changjiang estuary in dry season from 2015 to 2017. Journal of East China Normal University. 2, 160-169. [in Chinese with English abstract].

Li, L., Zhu, J.R., Wu, H., 2012. Impacts of wind stress on saltwater intrusion in the Yangtze Estuary. Science China Earth Sciences, 55 (7), 1178-1192. https://dx.doi.org/10.1007/s11430-011-4311-1.

Li, L., Zhu, J.R., Wu, H., Guo, Z.G., 2014. Lateral saltwater intrusion in the North Channel of the Changjiang Estuary. Estuaries and coasts, 37 (1), 36-55. https://dx.doi.org/10.1007/s12237-013-9669-1.

Li, L., Zhu, J.R., Wu, H., Wang, B., 2010. A numerical study on water diversion ratio of the Changjiang (Yangtze) estuary in dry season. Chinese Journal of Oceanology and Limnology, 28 (3), 700-712. https://dx.doi.org/10.1007/s00343-010-9114-2.

Lyu, H.H., Zhu, J.R., 2018a. Impacts of Tidal Flat Reclamation on Saltwater Intrusion and Freshwater Resources in the Changjiang Estuary. Journal of Coastal Research, 35(2),

689 314-321. https://jstor.org/stable/26626840.
690 Lyu, H.H., Zhu, J.R., 2018b. Impact of the bottom drag coefficient on saltwater intrusion in the
691 extremely shallow estuary. Journal of Hydrology, 557, 838-850.
692 https://doi.org/10.1016/j.jhydrol.2018.01.010.
693 Mellor, G.L., Yamada, T., 1982. Development of a turbulence closure model for geophysical
694 fluid problems. Reviews of Geophysics, 20 (4), 851-875.
695 https://doi.org/10.1029/RG020i004p00851.
696 Prandle, D., 1985. On salinity regimes and the vertical structure of residual flows in narrow
697 tidal estuaries. Estuarine, Coastal and Shelf Science, 20(5), 615-635.
698 https://dx.doi.org/10.1016/0272-7714(85)90111-8.
699 Prandle, D., 2006. Dynamical controls on estuarine bathymetry: assessment against UK
700 database. Estuar. Coast. Shelf Sci. 68 (1-2), 282-288.
701 https://dx.doi.org/10.1016/j.ecss.2006.02.009.
702 Prandle, D., Lane, A., 2015. Sensitivity of estuaries to sea level rise: Vulnerability
703 indices. Estuarine, Coastal and Shelf Science, 160, 60-68.
704 https://dx.doi.org/10.1016/j.ecss.2015.04.001.
705 Pritchard, D.W., 1956. The dynamic structure of a coastal plain estuary. J Marine Res, 33-42.
706 Qiu, C., Zhu, J.R., 2013. Influence of seasonal runoff regulation by the Three Gorges Reservoir
707 on saltwater intrusion in the Changjiang River Estuary. Continental Shelf Research, 71,
708 16-26. https://dx.doi.org/10.1016/j.csr.2013.09.024.
709 Qiu, C., Zhu, J.R., 2015. Assessing the influence of sea level rise on salt transport processes and
710 estuarine circulation in the Changjiang River estuary. Journal of Coastal Research, 31 (3),
711 661-670. https://www.bioone.org/doi/abs/10.2112/JCOASTRES-D-13-00138.1.

712 Qiu, C., Zhu, J.R., Gu, Y.L., 2012. Impact of seasonal tide variation on saltwater intrusion in the
713 Changjiang River estuary. Chinese Journal of Oceanology and Limnology, 30 (2), 342-351.
714 https://dx.doi.org/10.1007/s00343-012-1115-x.
715 Shen, H.T., Mao, Z.C., Zhu, J.R., 2003. Saltwater intrusion in the Changjiang Estuary. Beijing:
716 China Ocean. [in Chinese with English abstract].
717 Simm, J.D., Beech, N.W., John, S., 1996. A manual for beach management. In Coastal
718 Management: Putting Policy Into Practice: Proceedings of the Conference Organized by
719 the Institution of Civil Engineers and Held in Bournemouth on 12-14 November 1995 (p.
720 229). Thomas Telford.
721 Simpson, J.H., Brown, J., Matthews, J., Allen, G., 1990. Tidal straining, density currents, and
722 stirring in the control of estuarine stratification. Estuaries, 13(2), 125-132.
723 https://dx.doi.org/10.2307/1351581.
724 Simpson, J.H., Hunter, J.R., 1974. Fronts in the Irish Sea. Nature 250, 404-406.
725 Willmott, C. J., 1981. On the validation of models. Physical geography, 2(2), 184-194.
726 https://dx.doi.org/10.1080/02723646.1981.10642213.
727 Wu, H., Shen, J., Zhu, J.R., Zhang, J., Li, L., 2014. Characteristics of the Changjiang plume and
728 its extension along the Jiangsu Coast. Continental Shelf Research, 76(2), 108-123.
729 https://doi.org/10.1016/j.csr.2014.01.007.
730 Wu, H., Zhu, J.R., 2007. Analysis of the transport mechanism of the saltwater spilling over
731 from the North Branch in the Changjiang Estuary in China. Acta Oceanologica Sinica, (1),
732 17-25. [in Chinese with English abstract].
733 Wu, H., Zhu, J.R., 2010. Advection scheme with 3rd high-order spatial interpolation at the
734 middle temporal level and its application to saltwater intrusion in the Changjiang Estuary.

735 Ocean Modelling, 33 (1), 33-51. https://dx.doi.org/10.1016/j.ocemod.2009.12.001.
736 Wu, H., Zhu, J.R., Chen, B.R., Chen, Y.Z., 2006. Quantitative relationship of runoff and tide to
737 saltwater spilling over from the North Branch in the Changjiang Estuary: A numerical
738 study. Estuarine Coastal Shelf Science, 69 (1-2), 125-132.
739 https://dx.doi.org/10.1016/j.ecss.2006.04.009.
740 Wu, H., Zhu, J.R., Choi, B. H., 2010. Links between saltwater intrusion and subtidal circulation
741 in the Changjiang Estuary: a model-guided study. Continental Shelf Research, 30 (17),
742 1891-1905. https://dx.doi.org/10.1016/j.csr.2010.09.001.
743 Zheng, L.Y., Chen, C.S., Liu, H.D., 2003. A modeling study of the Satilla River Estuary,
744 Georgia. I: Flooding-drying process and water exchange over the salt marsh-estuary-shelf
745 complex. Estuaries, 26 (3), 651-669. https://doi.org/10.1007/BF02711977.
746 Zheng, L.Y., Chen, C.S., Zhang, F.Y., 2004. Development of water quality model in the Satilla
747 River Estuary, Georgia. Ecological modelling, 178 (3-4), 457-482.
748 https://doi.org/10.1016/j.ecolmodel.2004.01.016.
749 Zhu, J.R., 2003. Ocean numerical calculation method and numerical model. Beijing: China
750 Ocean Press. [in Chinese with English abstract].
751 Zhu, J.R., Bao, D.Y., 2016. The effects of river regime changes in the Changjiang Estuary on
752 hydrodynamics and salinity intrusion in the past 60 years I. River regime changes.
753 Haiyang Xuebao, 38 (12), 11-22. https://doi.org/10.3969/j.issn.0253-4193.2016.12.0012.
754 Zhu, J.R., Ding, P.X., Zhang, L.Q., Wu, H., Cao, H.J., 2006. Influence of the deep waterway
755 project on the Changjiang Estuary. In The environment in Asia Pacific harbours (pp.
756 79-92). Springer Netherlands. https://dx.doi.org/10.1007/1-4020-3655-8_6.
757 Zhu, J.R., Gu, Y.L., Wu, H., 2013. Determination of the period not suitable for taking domestic

758 water supply to the Qingcaosha Reservoir near Changjiang River Estuary. Oceanologia et
759 Limnologia Sinica, 44(5), 1138-1145. [in Chinese with English abstract].
760 Zhu, J.R., Wu, H., 2013. Numerical simulation of the longest continuous days unsuitable for
761 water intake in the Dongfengxisha Reservoir of the Changjiang Estuary. Journal of East
762 China Normal University (Natural Science), 5, 1-8. [in Chinese with English abstract].
763 Zhu, J.R., Wu, H., Li, L., 2015. Hydrodynamics of the Changjiang Estuary and Adjacent Seas.
764 In Ecological Continuum from the Changjiang (Yangtze River) Watersheds to the East
765 China Sea Continental Margin (pp. 19-45). Springer International Publishing.
766 https://dx.doi.org/10.1007/978-3-319-16339-0_2.
767 Zhu, J.R., Wu, H., Li, L., Wang, B., 2010. Saltwater intrusion in the Changjiang Estuary in the
768 extremely drought hydrological year 2006. Journal of East China Normal University
769 (Natural Science), 4 (1), 1-6. [in Chinese with English abstract].